# Supporting Information

# Assembly of new organic-inorganic hybrids based on copper-bis(triazole) complexes and Keggin-type polyoxometalates with different negative charges

**Xiu-Li Hao,[a] Yuan-Yuan Ma,[a] Chen Zhang,[a] Qian Wang,[a] Xin Cheng,[a] Yong-Hui Wang,*[a] Yang-Guang Li*[a] and En-Bo Wang[a]**

## Contents

## 1. Additional structural figures for compound 1

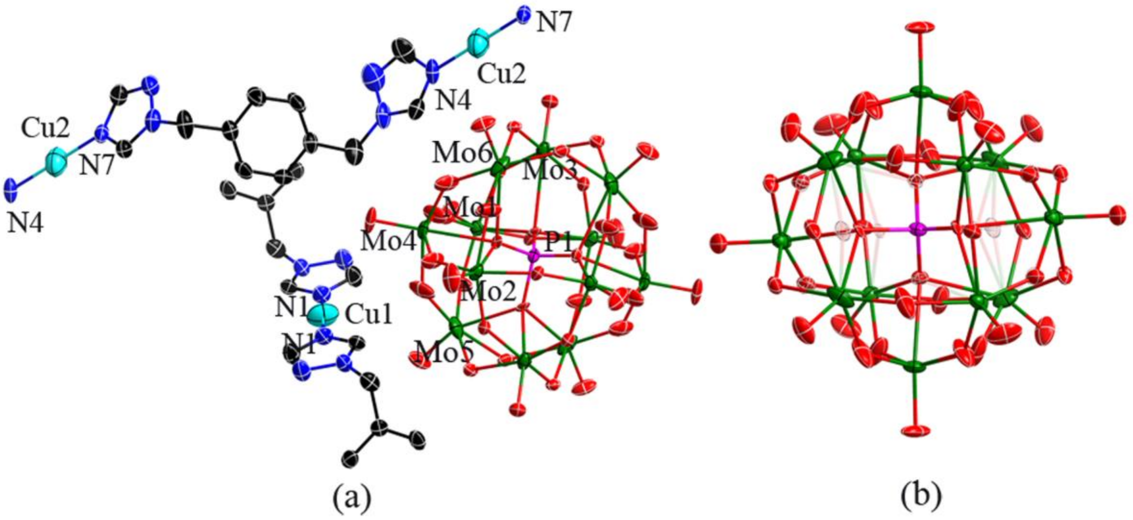

**Fig. S1** (a) ORTEP diagram of the basic structural units in **compound 1** with thermal ellipsoids at 30% probability displacement. All H atoms and solvent molecules are omitted for clarity. (b) Disorder of $PO_4$ in **compound 1**.

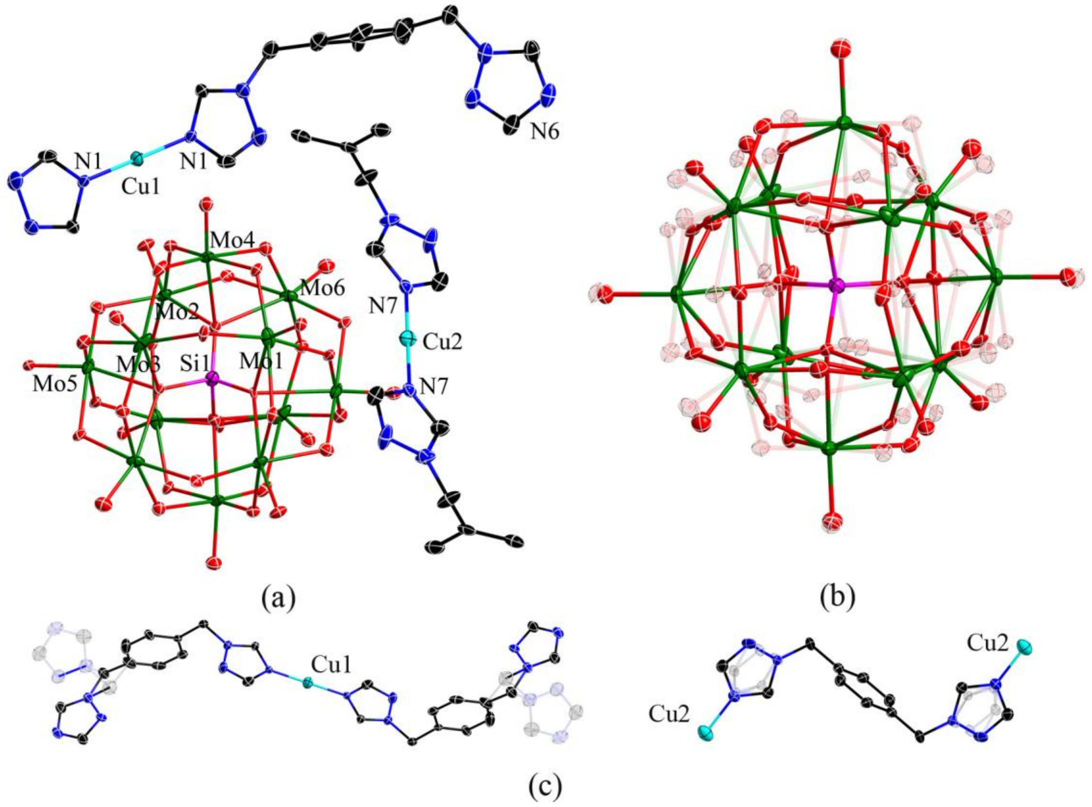

**Fig. S2** ORTEP diagram of the basic structural units in **compound 2** with thermal ellipsoids at 30% probability displacement. All H atoms and solvent molecules are omitted for clarity. (b) Disorder of $PO_4$ and all the O atoms in **compound 2**. (c) Disorder of part of the C and N atoms in organic ligands of **compound 2**.

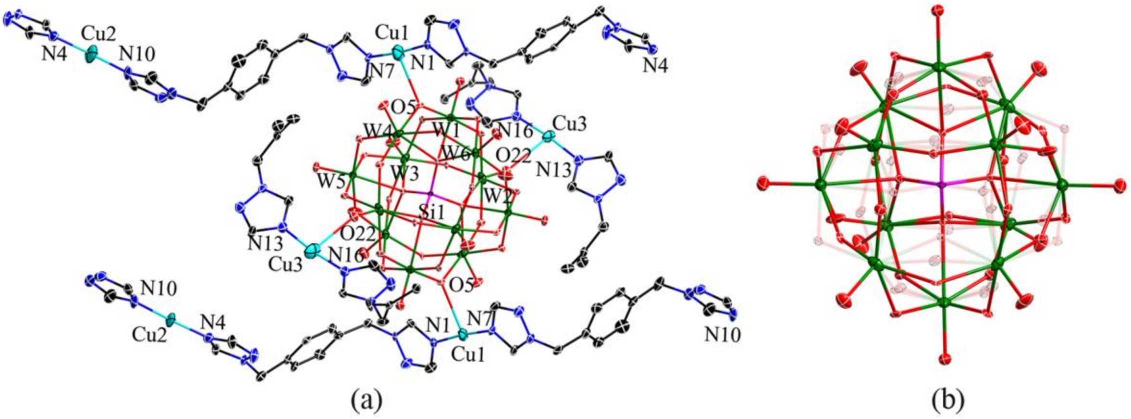

(a) (b)

**Fig. S3** (a) ORTEP diagram of the basic structural units in **compound 3** with thermal ellipsoids at 30% probability displacement. All H atoms and solvent molecules are omitted for clarity. (b) Disorder of $PO_4$ and part of the O atoms in **compound 3**.

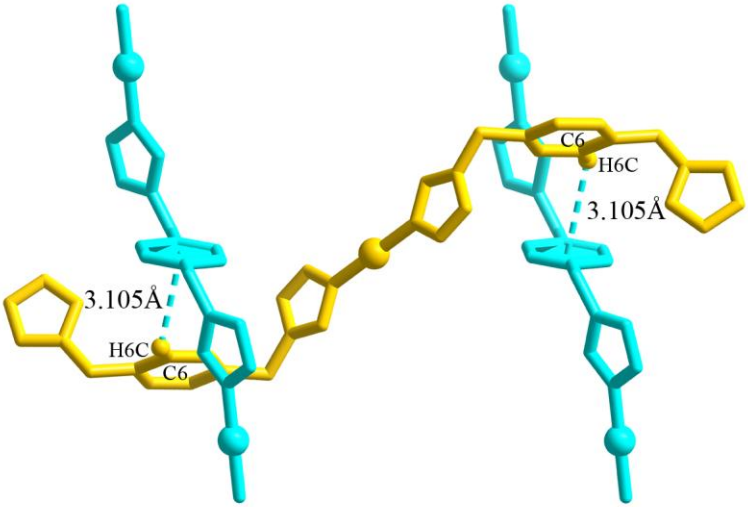

**Fig. S4** The typical C-H-π interactions between infinite 1D chains and finite 1D chains supramolecular nets in **2.**

## **2.** Selected bond lengths and angles for compounds **1-3**

**Table S1**. Selected bond lengths (Å) and angles (deg) of **1**.

| | | | |
|---|---|---|---|
| Cu(1)-N(1)#1 | 1.849(5) | Cu(1)-N(1) | 1.849(5) |
| Cu(2)-N(4) | 1.863(6) | Cu(2)-N(7) | 1.875(6) |
| N(1)#1-Cu(1)-N(1) | 180.000(1) | N(4)-Cu(2)-N(7) | 179.0(3) |

Symmetry transformations used to generate equivalent atoms: #1 -x,-y,-z+1 #2 -x+2,-y+2,-z #3 -x+1,-y+1,-z+1 #4 x,y,z+1 #5 x,y,z-1

**Table S2**. Selected bond lengths (Å) and angles (deg) of **2**.

| | | | |
|---|---|---|---|
| Cu(1)-N(1) | 1.876(11) | Cu(1)-N(1)#3 | 1.876(11) |
| Cu(2)-N(7)#4 | 1.84(2) | Cu(2)-N(7A) | 2.03(3) |
| Cu(2)-N(7) | 1.84(2) | Cu(2)-N(7A)#4 | 2.03(3) |
| N(1)-Cu(1)-N(1)#3 | 180.0(6) | N(7)-Cu(2)-N(7A)#4 | 173.8(12) |
| N(7)-Cu(2)-N(7)#4 | 180.0 | N(7)#4-Cu(2)-N(7A)#4 | 6.2(12) |
| N(7)-Cu(2)-N(7A) | 6.2(12) | N(7A)-Cu(2)-N(7A)#4 | 180.0 |
| N(7)#4-Cu(2)-N(7A) | 173.8(12) | | |

Symmetry transformations used to generate equivalent atoms: #1 -x+1,-y,-z+1 #2 x,y-1,z #3 -x-1,-y,-z+2 #4 -x+1,-y+1,-z+1 #5 x,y+1,z #6 -x+1,-y+1,-z+2

**Table S3**. Selected bond lengths (Å) and angles (deg) of **3**.

| | | | |
|---|---|---|---|
| Cu(1)-N(7) | 1.902(7) | Cu(1)-O(5) | 2.533(1) |
| Cu(1)-N(1) | 1.906(7) | Cu(2)-N(4) | 1.909(7) |
| Cu(2)-N(10)#2 | 1.902(8) | Cu(3)-N(13) | 1.921(7) |
| Cu(3)-N(16) | 1.914(7) | Cu(3)-O(22) | 2.644(1) |
| N(7)-Cu(1)-N(1) | 174.7(3) | N(1)-Cu(1)-O(5) | 91.7(2) |
| N(7)-Cu(1)-O(5) | 92.8(8) | N(10)#2-Cu(2)-N(4) | 176.5(4) |
| N(16)-Cu(3)-O(22) | 87.5(3) | N(13)-Cu(3)-O(22) | 87.5(1) |
| N(16)-Cu(3)-N(13) | 174.3(3) | | |

Symmetry transformations used to generate equivalent atoms: #1 -x,-y+1,-z+2 #2 x+1,y-1,z+1 #3 x-1,y+1,z-1 #4 -x+2,-y+1,-z+1 #5 -x+1,-y,-z+2

Table S4 The bond valence sum calculations of W for compound 3

| | Compound3 |
|---|---|
| W1 | 5.550 |
| W2 | 6.001 |
| W3 | 5.428 |
| W4 | 5.700 |
| W5 | 6.174 |
| W6 | 6.164 |
| $W_{average}$ | 5.836 |

## **3.** Additional measurements for compounds **1-3**

### **3.1** XPS spectra

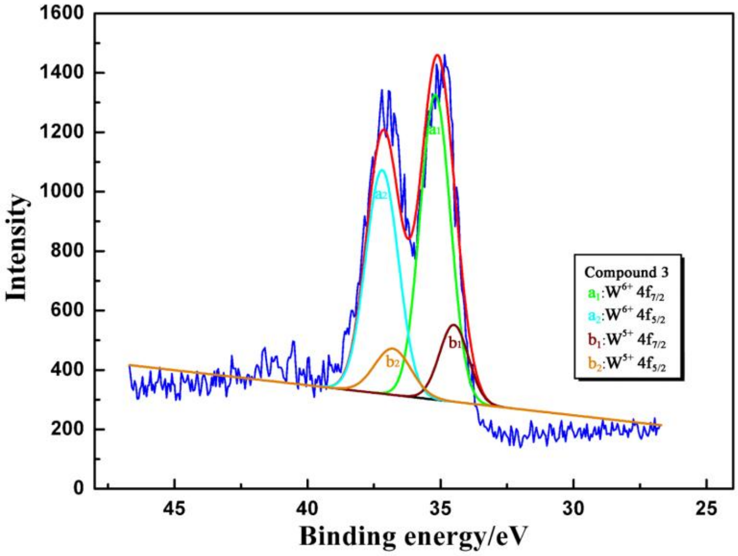

**Fig. S5** XPS spectra of W4f level of compound **3**. The XPS of **3** show four partially overlapped peaks, and the fit of curve provides with positions of these four peaks at 34.5, 35.2, 36.8 and 37.2 eV attributing to $W^{V}$ $4f_{7/2}$, $W^{VI}$ $4f_{7/2}$, $W^{V}$ $4f_{5/2}$ and $W^{VI}$ $4f_{5/2}$, respectively. The ratios of the peak are for $W^{V}$ to $W^{VI}$ is ca. 2 : 10.

## **3.2** Cyclic voltammograms

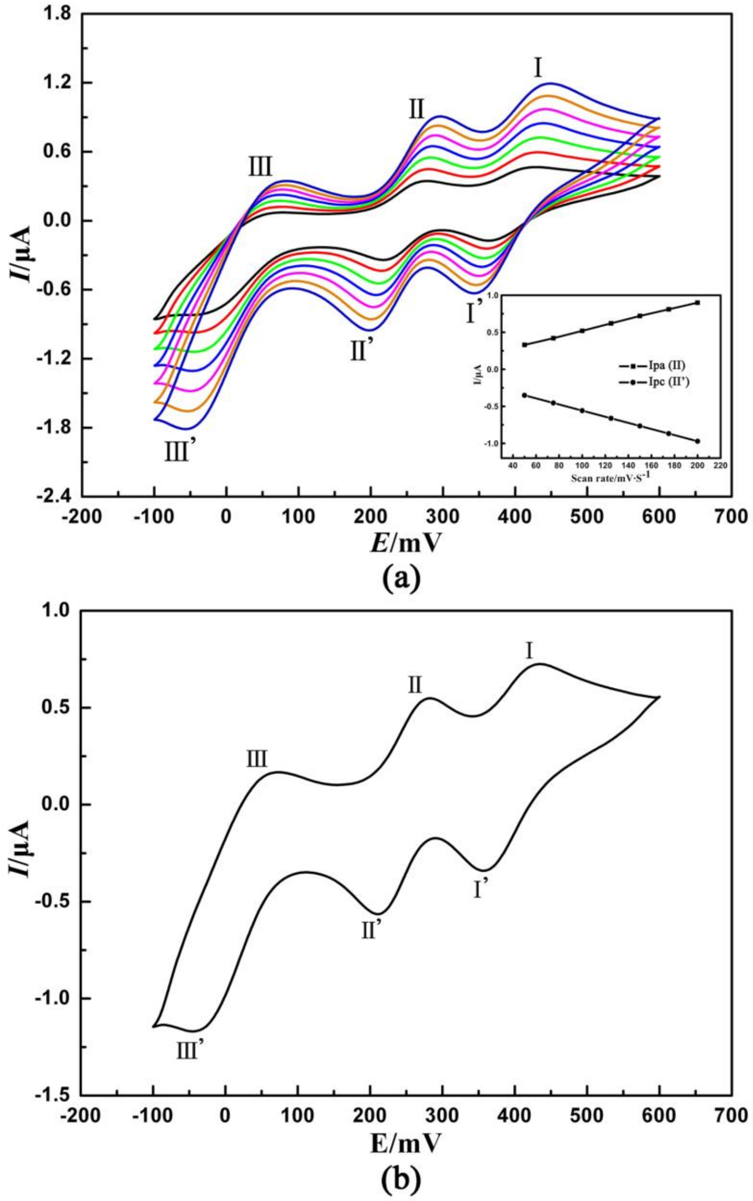

**Fig. S6 (a)** The cyclic voltammograms (CV) of **1-CPE** in 1 M $H_2SO_4$ at different scan rates (from inner to outer: 50, 75, 100, 125, 150, 175, and 200 mV/s). The inset shows plots of the dependence of anodic peak and cathodic peak (II-II’) current on scan rates. **(b)** Cyclic voltammogram of **1-**CPE in a 1 M $H_2SO_4$ solution at a scan rate of 100 mV/s; the reference electrode was Ag/AgCl.

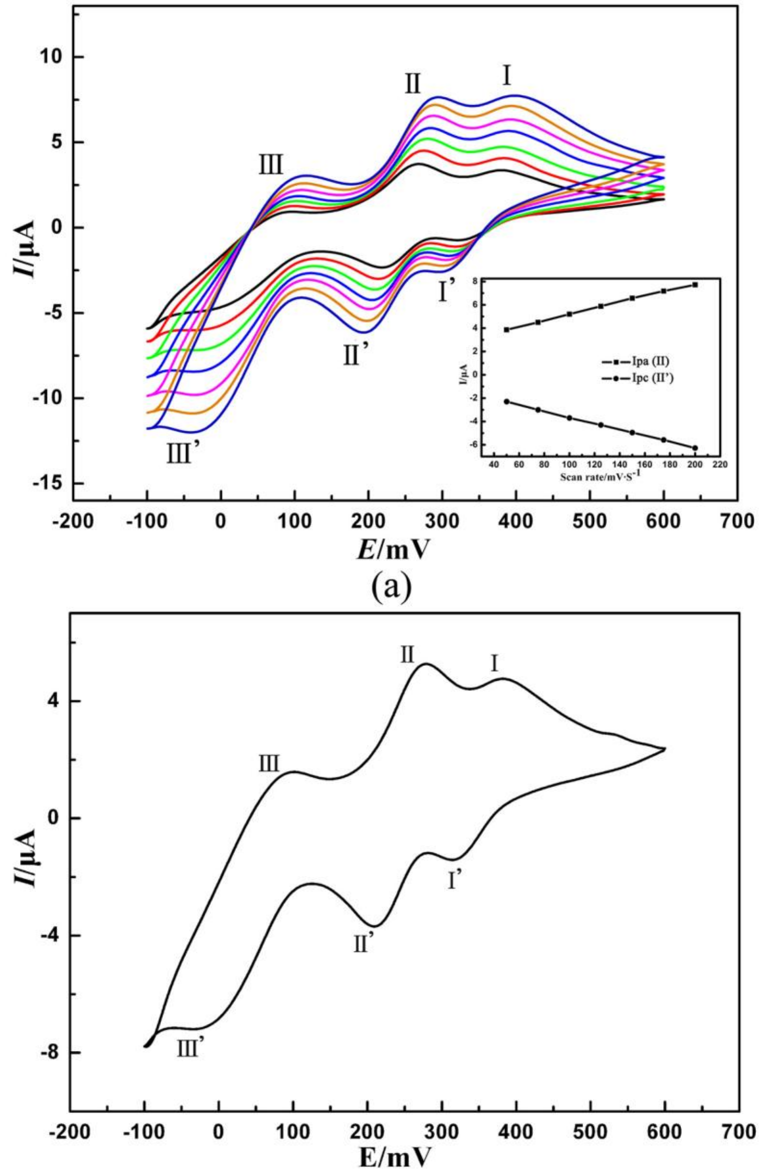

(a)

(b)

**Fig. S7 (a)** The cyclic voltammograms (CV) of **2-CPE** in 1 M $H_2SO_4$ at different scan rates (from inner to outer: 50, 75, 100, 125, 150, 175, and 200 mV/s). The inset shows plots of the dependence of anodic peak and cathodic peak (II-II') current on scan rates. **(b)** Cyclic voltammogram of **2-**CPE in a 1 M $H_2SO_4$ solution at a scan rate of 100 mV/s; the reference electrode was Ag/AgCl.

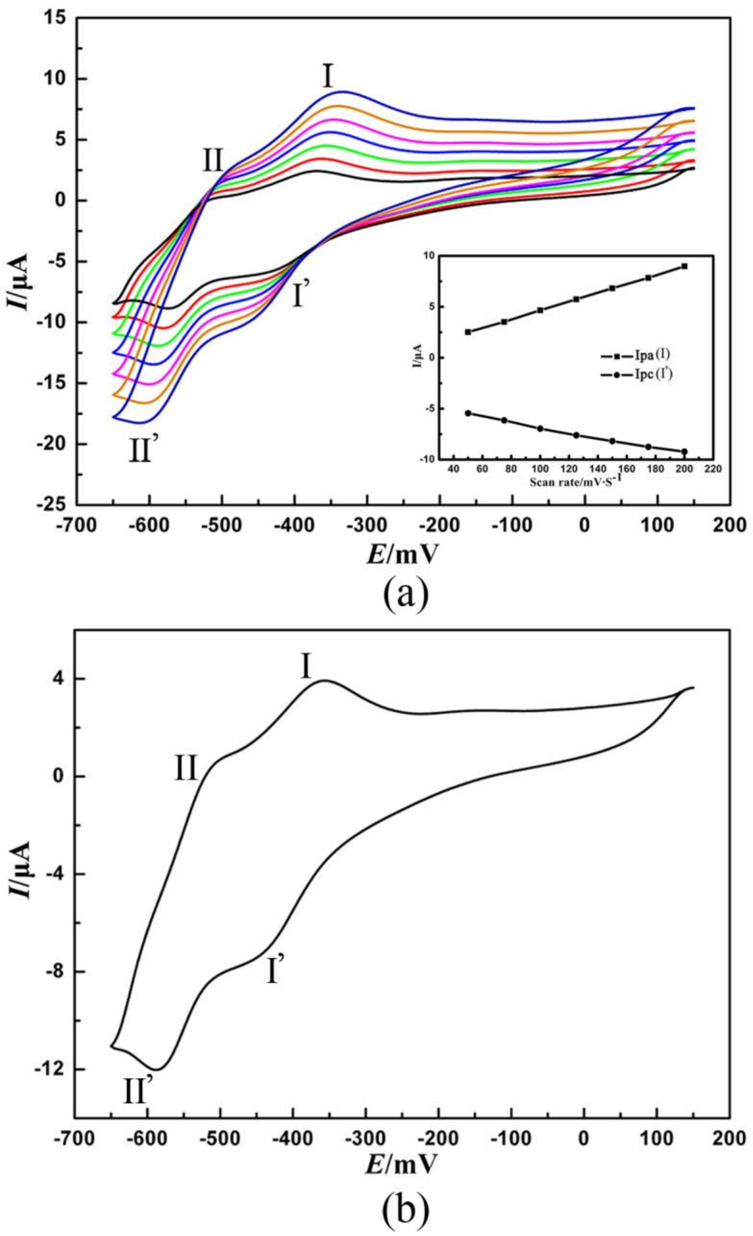

**Fig. S8 (a)** The cyclic voltammograms (CV) of **3-CPE** in 1 M $H_2SO_4$ at different scan rates (from inner to outer: 50, 75, 100, 125, 150, 175, and 200 mV/s). The inset shows plots of the dependence of anodic peak and cathodic peak (I-I') current on scan rates. **(b)** Cyclic voltammogram of **3-**CPE in a 1 M $H_2SO_4$ solution at a scan rate of 100 mV/s; the reference electrode was Ag/AgCl.

### **3.3** IR spectra

In the IR spectrum of compound **1** (Fig. S9), four characteristic peaks of $[PMo_{12}O_{40}]^{3-}$ are observed in the range of 1000-700 cm$^{-1}$. The peaks at 1062 cm$^{-1}$, 956 cm$^{-1}$, 865 cm$^{-1}$, and 802 cm$^{-1}$ are ascribed to the vibrations of *v*(P-O), *v*(Mo=Od) and *v*(Mo–Ob/c–Mo), respectively. In the IR spectrum of **2** (Fig. S10), the characteristic peaks for *v*(Si-O), *v*(Mo=Od) and *v*(Mo–Ob/c–Mo) of the polyoxoanion occur at 991 cm$^{-1}$, 951 cm$^{-1}$, 904 cm$^{-1}$, and 786 cm$^{-1}$. The IR spectrum of compound **3** is shown in Fig. S11. In the spectrum, characteristic bands at 1007 cm$^{-1}$, 948 cm$^{-1}$, 901 cm$^{-1}$, and 791 cm$^{-1}$ are attributed to v(Si–O), v(W=Od) and v(W–Ob/c–W), respectively. In addition, for three compounds, the peaks at ca. 3118 cm$^{-1}$ are attributed to the vibrations of the *v*(C-H) in phenyl and pyridyl rings of BBTZ ligand. Peaks in the regions of 1631-1425 cm$^{-1}$ may belong to the vibrations of the *v*(C=C), *v*(C=N) and *v*(C=N) in phenyl and triazole rings of BBTZ ligand in **1-3**. The peaks at ca. 3431 cm$^{-1}$ are attributed to the vibrations of *v*($H_2O$).

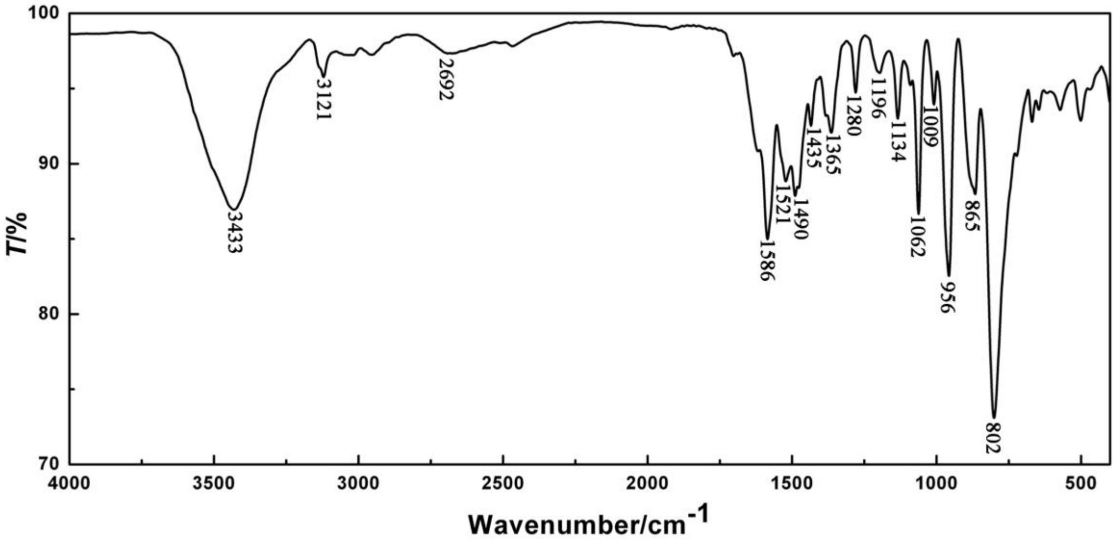

**Fig. S9** IR spectrum of compound **1**.

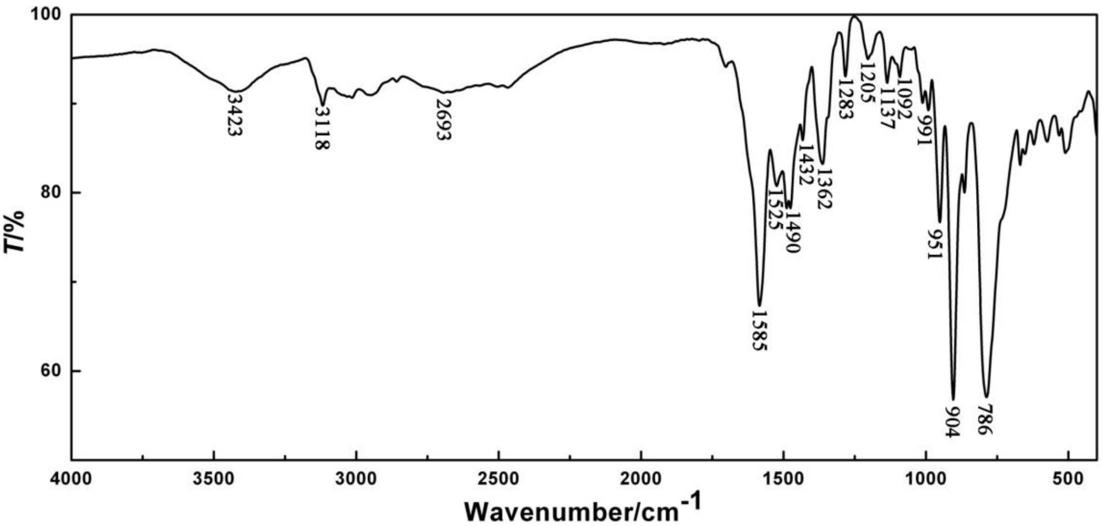

**Fig. S10** IR spectrum of compound **2**.

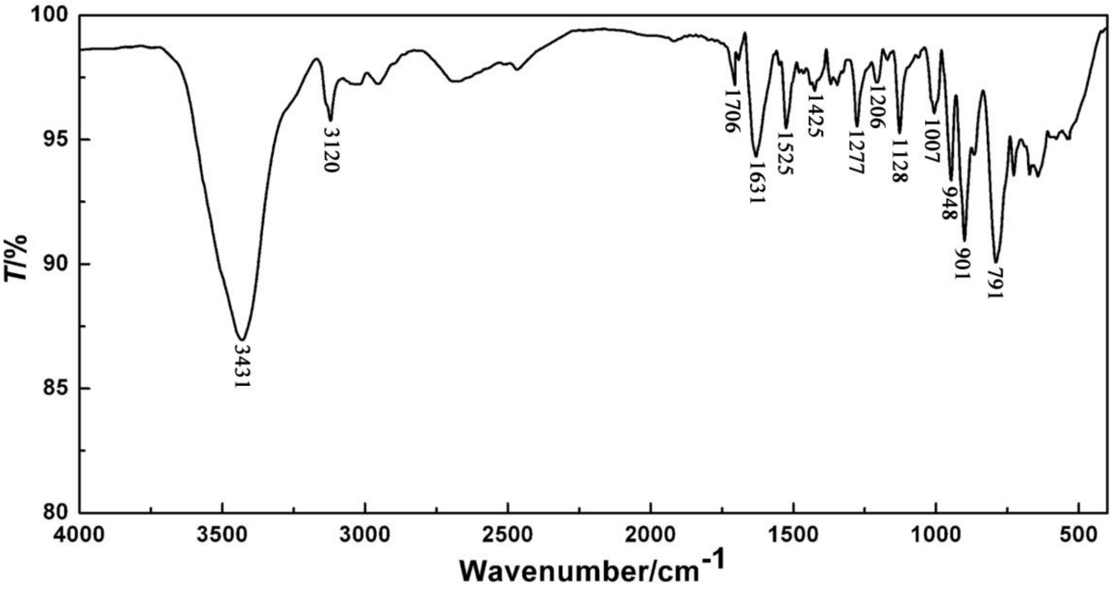

**Fig. S11** IR spectrum of compound **3**.

### **3.4** TG Analyses

The TG curve of compound **1** shows one weight loss steps (Fig. S12). The whole weight loss of 26.43 % occurring from 310 to 495 °C is mainly ascribed to the decomposition and loss of BBTZ ligands in **1** (calcd. 26.34 %).

The TG curve of compound **2** (Fig. S13) shows the first weight loss of 1.53% in the temperature range of 65-110 $^{o}$C corresponding to two and a half lattice water molecules and three coordinated water molecules (calculated value 1.66%). The second weight loss of 26.85 % from 290 to 550 °C is ascribed to decomposition and loss of BBTZ ligands (calcd. 26.60%). The whole weight loss of 28.38% is in agreement with the calculated value 28.26%.

The TG curve of compound **3** also shows two continuous weight loss steps (Fig. S14). The first weight loss of 0.65 % in the temperature range of 55 ~ 80 °C corresponds to the loss of solvent acetonitrile and water molecules as well as five coordinated water molecules (calcd. 0.76%). The second weight loss in the range of 220 ~ 553 °C is 30.55% and attributed to the loss of BBTZ ligands (calcd. 30.42%). The whole weight loss of 31.20 % is in agreement with the calculated value 31.18%.

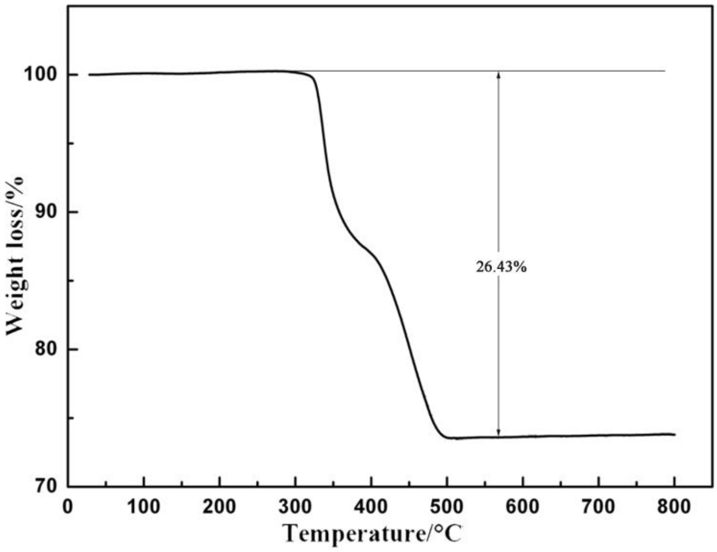

**Fig. S12** TG curve of compound **1**.

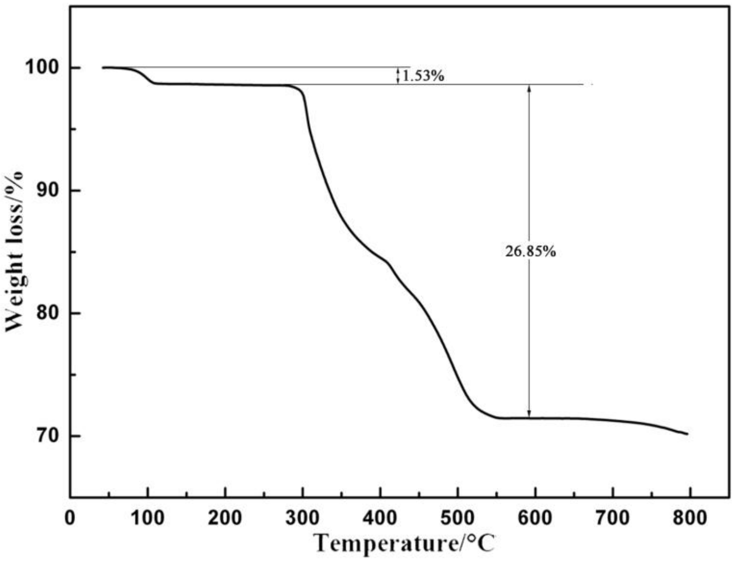

**Fig. S13** TG curve of compound **2**.

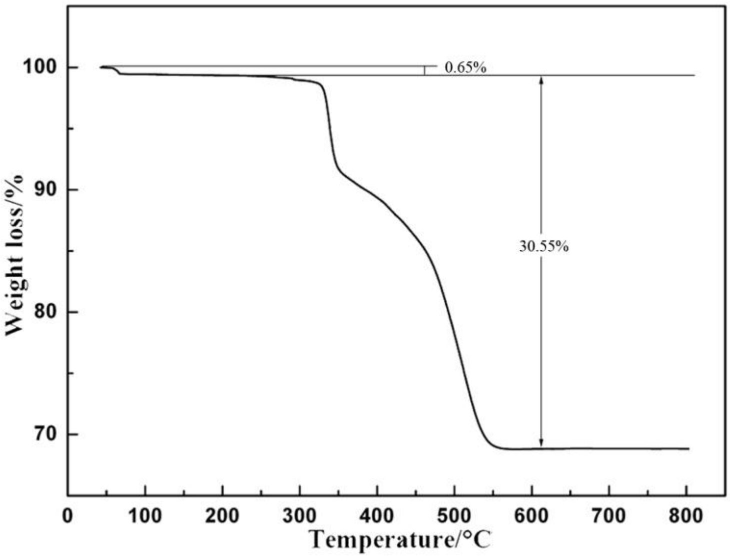

**Fig. S14** TG curve of compound **3**.

**3.5** Powder X-ray diffractions

In order to check the phase purity of compounds **1**-**3**, the PXRD patterns of them were recorded at room temperature. As shown in Figs. S15-S17, the peak positions of simulated and experimental patterns of compounds **1**-**3** are in agreement with each other, indicating the good phase purity of them. The differences in intensity are due to the preferred orientations of the crystalline powder samples.

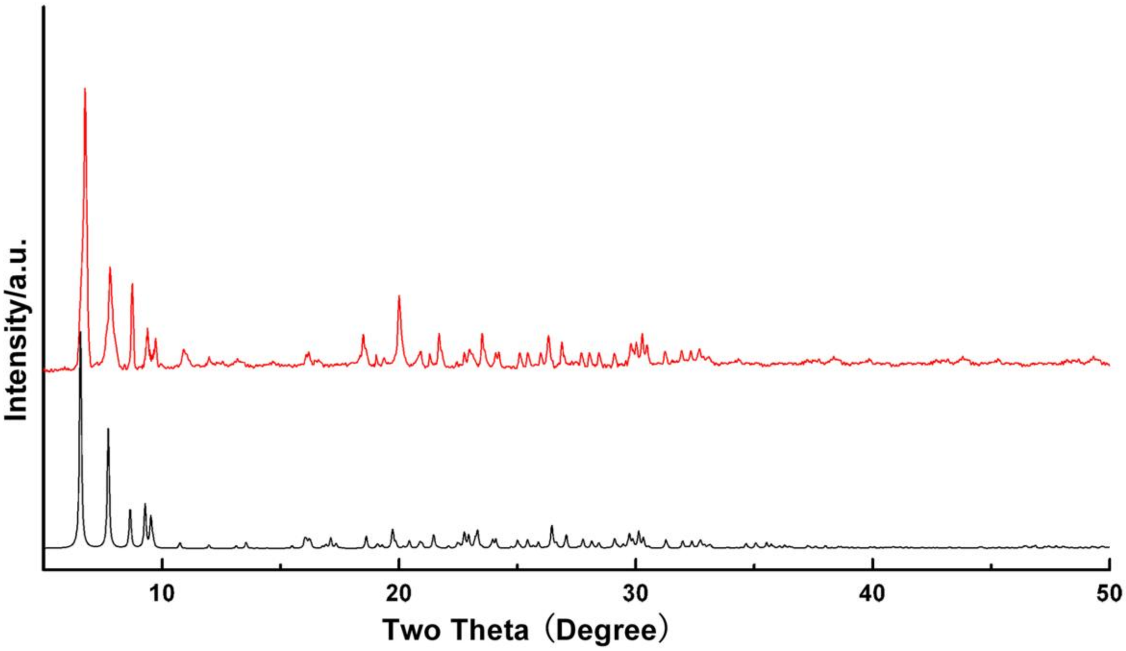

**Fig. S15** Measured (red) and simulated (black) XRD patterns of compound **1**.

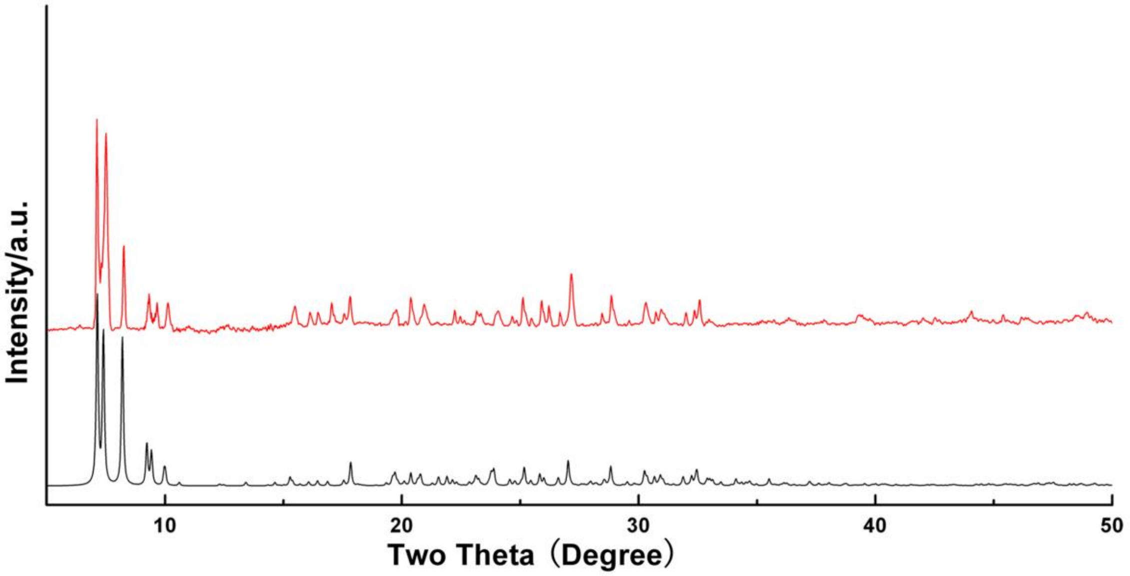

**Fig. S16** Measured (red) and simulated (black) XRD patterns of compound **2**.

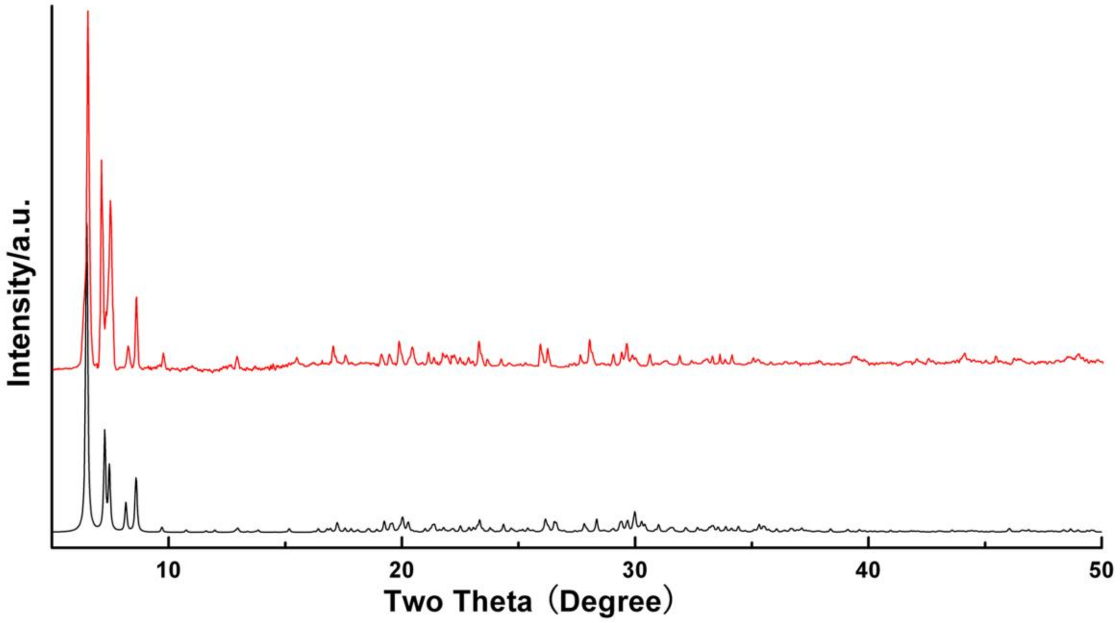

**Fig. S17** Measured (red) and simulated (black) XRD patterns of compound **3**.